Clemson University

TigerPrints

12-2023

Temperature Gradient Effect on Solid-Liqid Interface Properties of Al-Cu Alloy: A Molecular Dynamics Study

Prashant Kumar Jha
Clemson University, jha5@g.clemson.edu

Follow this and additional works at: https://tigerprints.clemson.edu/all_theses

Part of the Manufacturing Commons, Metallurgy Commons, and the Other Materials Science and Engineering Commons

TEMPERATURE GRADIENT EFFECT ON SOLID-LIQID INTERFACE
PROPERTIES OF Al-Cu ALLOY: A MOLECULAR DYNAMICS STUDY

A Thesis
Presented to
the Graduate School of
Clemson University

In Partial Fulfillment
of the Requirements for the Degree
Master of Science
Mechanical Engineering

---

by
Prashant Kumar Jha
December 2023

Accepted by:
Dr. Enrique Martinez Saez, Committee Chair
Dr. Garret Pataky
Dr. Sun Cheng

ABSTRACT

Aluminum-copper (Al-Cu) alloys are widely used in the aerospace industry due to their favorable strength-to-weight ratio, good fatigue resistance, and corrosion resistance. These properties make Al-Cu alloys an excellent choice for aircraft structural components that require high strength and low weight. Additive manufacturing (AM), also known as 3D printing, has emerged as a promising processing method for Al-Cu alloys in aerospace manufacturing. AM enables the production of lightweight optimized geometries difficult to manufacture through conventional subtractive methods. AM also reduces material waste by only depositing material where needed in the part geometry. The rapid solidification conditions in AM processes motivate further study of solid-liquid interface properties in Al-Cu alloys. This work examines the solid-liquid interface using molecular dynamics (MD) simulations and the capillary fluctuation method (CFM). CFM facilitates quantitatively determining key interfacial characteristics like stiffness, energy, and anisotropy. Simulations were performed under both equilibrium conditions and applied thermal gradients to replicate AM processes. Applying a thermal gradient across the interface led to an augmentation in stiffness and interfacial free energy while preserving the constancy of anisotropic characteristics. This phenomenon was theoretically elucidated by employing a Taylor expansion of the interfacial free energy function. The equations representing the relationships are: $\gamma_{(\theta,G)} = \mu G + \gamma_0$ for energy and $S_{(\theta,G)} = \gamma + \gamma_{\theta\theta} + \mu G$ for stiffness, where G represents the thermal gradient. The present study involved simulations on Al-Cu alloys containing varying concentrations of copper, specifically 2%, 3.58%, and 5.065% Cu. These simulations were conducted at different

temperatures, 905K, 888K, and 874K, respectively. A total of eight unique interface orientations were investigated. The obtained results were consistent with the proposed theoretical relationships, thereby confirming the presence of anisotropy independent of the gradient and the validity of the first-order Taylor expansion. This study provides fundamental insights into interfacial phenomena during Al-Cu alloy solidification, which can help optimize AM processes by reducing defects. The calculated parameters have significant implications for larger scale computational models of AM by improving accuracy compared to experiments when incorporating non-equilibrium conditions.

DEDICATION

To my parents, for supporting and always believing in me and Dr. Enrique Martinez Saez

for giving me this opportunity.

ACKNOWLEDGMENTS

TABLE OF CONTENTS

LIST OF TABLES

LIST OF FIGURES

CHAPTER ONE

This chapter covers the shortcomings of the current analytic models and the goal of the research being presented. Using Molecular Dynamic simulation, rapid solidification for metal alloys at the atomic scale is investigated. The rapid rise of additive manufacturing and mechanisms for metal joining failure in interface development spurred this research.

1.1 Motivation

The properties and behavior of solid-liquid interfaces are of great scientific and industrial importance. Gaining a predictive understanding of interface phenomena during rapid solidification processes like welding, additive manufacturing, and casting is critical for optimizing manufacturing techniques and performance outcomes. However, modeling the intricate atomic-level dynamics at solidification fronts remains extremely challenging. The main goal is to explore the growth morphologies and microstructure evolution at interfaces during rapid solidification of Al-Cu alloy, taking into account the influence of atomic processes. This knowledge can facilitate optimized computational modeling of defect formation, residual stress evolution, and alloy design for processes like additive manufacturing, laser welding, and ultrasonic consolidation. More reliable physics-based predictions of rapid solidification phenomena will accelerate development and deployment of new materials and structural components with superior performance and reliability.

1.2 Literature Review

Important in both material science and industry generally, solidification processing can be either normal or rapid. The substantial differences in characteristics and behaviors

1

between these two solidification modes have an impact on the final properties of the material. [1]

Normal solidification takes place when the solid-liquid interface velocity is comparatively low, producing a relatively smooth solidification front. The reason for this smoothness is that the microstructural characteristic length scale, which establishes the distance between grains or other structural elements within the solid material, is significantly smaller than the diffusion length scale, which represents the distance that atoms can migrate before they solidify. In essence, atoms have enough time to diffuse before the solid structure solidifies. A Péclet number less than 1 (a dimensionless parameter comparing heat transfer to diffusion rate) indicates this circumstance [2,3].

The product of the interface velocity and the tip radius square remains constant during normal solidification. This connection results from the fundamental idea that the rate of heat removal from the solidification front determines the rate of solidification. Because heat must be removed more quickly when the interface velocity is higher, a smaller tip radius is required for effective solidification.

On the other hand, rapid solidification happens when the interface velocity is extremely high, creating an irregular and complex solidification front. Since the diffusion length scale is much shorter than the microstructural characteristic length scale, this irregularity suggests that atoms did not have enough time to undergo extensive diffusion before solidifying. The Péclet number exceeds 1 in these circumstances.

There is a lower range where the interface can still be regarded as being in local equilibrium within the context of rapid solidification. The assumption of local interfacial

2

equilibrium, however, falters as the interface velocity rises. Due to the rapid solidification process, this departure from equilibrium causes non-equilibrium phenomena like solute trapping, in which solute atoms are concentrated at the front of the solidification process.

A visual representation of the changes in the solidification process is provided by Figure 1, which shows the variations in interfacial conditions that go along with different solidification velocities. These distinctions between normal solidification and rapid solidification are essential for comprehending and managing the properties of materials created through solidification processing, enabling customized results for particular applications in a range of industries, from metallurgy to electronics.
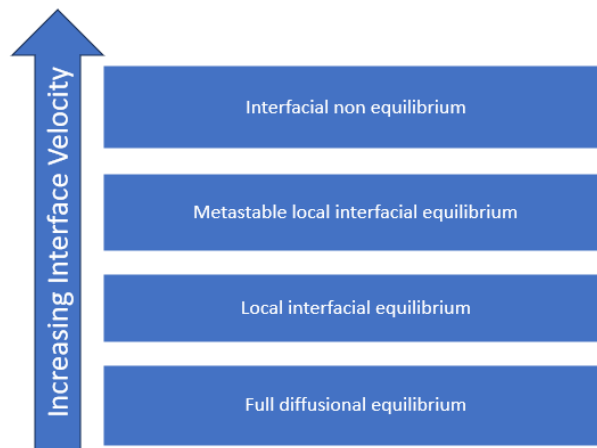
Figure 1: The alterations in the interfacial conditions occurring at the interface between a solid and a liquid as a consequence of the solidification velocity. [3]

During the solidification process, materials have the potential to develop dendrites, which are characterized by their branching, tree-like structures. In conventional solidification processes, such as welding, the formation of dendrites is primarily influenced by two crucial factors: the velocity of each dendrite tip and the interfacial stiffness of the

material [4-9]. Researchers have conventionally conducted the examination of growth patterns through the utilization of phase-field simulations. These simulations incorporate a Gibbs-Thomson condition based on equilibrium principles into their models. Furthermore, researchers reinforce their findings by combining experimental data and molecular dynamic (MD) simulations. Nevertheless, within the context of rapid solidification processes such as additive manufacturing, the formation of dendrites occurs in thermodynamic environments characterized by high dynamics. The crystal-melt interface, which delineates the boundary between a material's solid and liquid phases, is greatly influenced by the dynamic nature of the surrounding environment. The interface is driven into a non-equilibrium state by the persistent fluctuations in temperature and pressure, indicating a departure from a state of equilibrium. As a result, the growth rate of the solid phase exceeds the rate at which the liquid phase undergoes solidification. The existing phase-field simulations, initially developed for modeling systems in thermodynamic equilibrium, face challenges in accurately replicating the observed phenomena of dendrite growth.

In a two-dimensional context, the Gibbs-Thomson condition establishes a relationship between the temperature at the interface, T_i , and the deviation from the melting temperature, T_m, arising from the interface's curvature and velocity:

$$T_i = T_m - \frac{T_m}{L} \sum_{i=1,2} \left[\gamma(\hat{n}) + \frac{\partial^2 \gamma(\hat{n})}{\partial \theta_i^2} \right] \frac{1}{R_i} - \frac{V_n}{\mu(\hat{n})} \tag{1}$$

Here, L represents the latent heat, $\gamma(\hat{n})$ stands for the interfacial free energy, θ_i refers to the local angles between the normal direction n and the two principal directions, and R_i denotes the principal radii of curvature. The last two terms, V and μ, represent the normal velocity of the interface and the kinetic coefficient, respectively [6]. The Gibbs-Thomson condition defines the interfacial stiffness, $\gamma(\hat{n}) + \frac{\partial^2 \gamma(\hat{n})}{\partial \theta_i^2}$, under equilibrium conditions, where it remains independent of temperature variations.

However, recent studies involving solid-solid phase interactions, utilizing the capillary fluctuation method [10,11], have demonstrated that the interfacial stiffness does, in fact, depend on thermal conditions. Typically, the interfacial properties of the material are determined through MD simulations [12] or are obtained through fitting to experimental data.

The continuous growth model is one of the most well-known and frequently used models to explain solute trapping in rapid solidification. This model explains the complex interaction between the solid and liquid phases during solidification and sheds light on the distribution of solute atoms in the resulting microstructure. It is an effective tool for forecasting and comprehending growth patterns, dimensional properties, micro segregation phenomena, and the ensuing formation of secondary phases during the solidification process. These microstructural characteristics are crucial because they have a significant impact on the material's mechanical, thermal, and chemical properties after it has solidified. The performance and behavior of the material in practical applications are heavily influenced by the properties of the microstructure that is created during solidification and is influenced by solute trapping. This is especially important in fields like metallurgy and

5

materials science, where optimizing material properties is a primary goal. Through meticulous control of the solidification process, engineers and researchers seek to manipulate and optimize the microstructural features to satisfy particular performance criteria.

Using sophisticated computational modelling techniques to better understand solute trapping and its effects on microstructure. Phase field modelling is one of these effective methods. Due to its solid theoretical underpinning, close ties to non-equilibrium thermodynamics, and computational efficiency when compared to conventional interface tracking methods, this method has grown in popularity. Engineers and scientists can simulate and research complex microstructural phenomena that take place during solidification and solid-state transformations by using phase field modelling. We can find links between different manufacturing process variables and microstructural characteristics by using phase field modelling. This helps us understand the underlying physics of rapid solidification and also offers a useful way to tailor materials' properties and optimize processing conditions.

Rapid solidification can be seen in Additive manufacturing, more popularly known as 3D printing, is a ground-breaking innovation in modern manufacturing that has fundamentally changed the way we produce goods [13]. Unlike traditional manufacturing methods, which rely on material removal processes such as cutting, milling, or casting, additive manufacturing (AM) works on the principle of building three-dimensional objects by sequentially adding material, layer by layer. This distinguishing feature distinguishes

AM and opens up a world of possibilities that were previously unattainable through conventional means.

The advantages of additive manufacturing over traditional manufacturing techniques are significant, and they have fueled its adoption and continuous advancement. First and foremost, AM allows for the fabrication of highly intricate and complex shapes with relative ease. These complex geometries would be extremely difficult or impossible to produce using traditional methods. Furthermore, AM allows for the creation of objects with tailored properties, such as exceptional strength-to-weight ratios, making it highly appealing for industries that require lightweight, high-strength components.

The rapid evolution of additive manufacturing technologies has sparked a surge of interest and research in this field. One of the primary challenges confronting researchers is the creation of predictive simulations capable of accurately forecasting the properties of AM-produced components. These simulations are critical for optimizing additive manufacturing processes, ensuring that manufactured parts meet stringent specifications, and mitigating defects and inconsistencies.

Several research projects have been launched in order to advance the development of predictive simulations for AM. These investigations have heavily relied on computational techniques such as Finite Element Analysis (FEA). FEA is a numerical method that allows researchers to simulate and comprehend the complex behavior of materials under a wide range of loading conditions. FEA has demonstrated its versatility in the context of AM by effectively simulating a variety of additive manufacturing

processes, including Selective Laser Melting (SLM) and Fused Deposition Modelling (FDM).

LBM (Laser Beam Melting): The Pinnacle of Additive Manufacturing. LBM is a significant and notable subset of additive manufacturing technology that represents a pinnacle in the field [14]. LBM is notable for its ability to directly fabricate fully dense metal parts from digital data. This method eliminates the need for traditional casting or machining, allowing the manufacture of intricate, customized metal components with exceptional precision and structural integrity.

The process starts with a digital 3D model of the desired part's geometry. The digital design is then used to precisely direct a high-powered laser beam to selectively melt and fuse metallic powder or wire, layer by layer. This fine-grained control over the material deposition and melting processes ensures the production of fully dense, highly detailed metal components that meet stringent specifications.

In order to develop a conceptual comprehension of how these flaws originate from the rapid temperature variations that are intrinsic to Additive Manufacturing, it is crucial to conduct an in-depth analysis of the atomic-level material interface. An interface is the region of transition between two or more phases of a substance. When systems function under consistent temperature and pressure conditions, the Gibbs free energy G_i, which represents the system's energetic stability and the dominant phase, is an essential parameter to consider. The equation $G_i = H - TS$ characterizes Gibbs free energy. In this context, the symbols H, T, and S denote the enthalpy, absolute temperature, and entropy, respectively, of the system. $dG_i = 0$ defines equilibrium.

Within the framework of AM's intrinsic rapid heating and cooling cycle, the interface experiences dynamic motion and maintains an unstable state. As a result, the traditional phase-diagram methodology is insufficient in delineating it. The models of thermal fluctuations incorporate a temperature range within which the substance has the capability to transform into either a solid or liquid state, as visually represented in Figure 2.
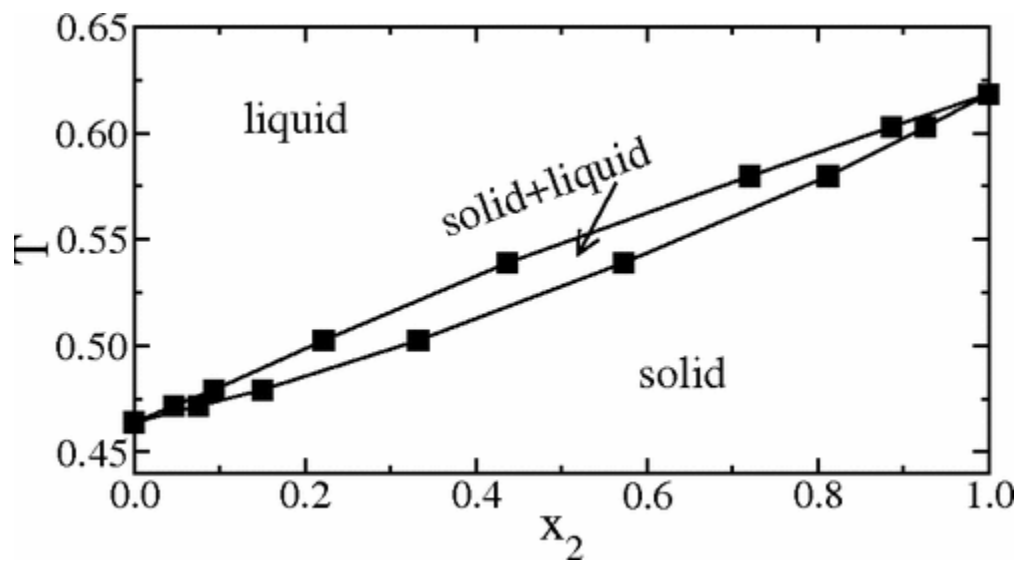
Figure 2: Temprature- composition phase diagram calculated for Lennard-Jones alloy [15]

The present study conducted in this dissertation places significant emphasis on the capillary fluctuation method and its utilization in the calculation of interfacial stiffness between two distinct phases.

1.3 Dissertation Structure

In Chapter 2, the subsequent sections of this dissertation provide a more comprehensive overview of materials, MD simulations, and methodologies. Additionally, this chapter explores some foundational principles to ensure that readers have the necessary

pre-existing knowledge to understand the research that is being presented. Chapter 3 provides an introduction to the simulation structures, describes the utilization of thermal gradient, and establishes the solid-liquid interface. It offers a thorough examination of these facets, supplying the reader with an in-depth comprehension of the methodology and its implementation. In Chapter 4, which functions as the concluding section, the accomplished objectives are succinctly reviewed and the contributions that have been delineated for the purpose of this work. Furthermore, an Appendix is provided to expound upon these contributions in greater detail and to suggest possible avenues for future research employing the analysis methods and approaches delineated in this dissertation.

Chapter Two

Methods and Materials

This section goes over material and method used in this study. Molecular Dynamics (MD) simulations, Capillary Fluctuation Method (CFM) and Anisotropy. MD is a popular computational method in material mechanics. It explains the fundamentals of MD simulations and how they relate statistical mechanics to practical mechanics. In a multi-scale computational approach, MD simulations play a critical role in providing material properties for larger-scale applications. CFM is a widely employed to express dynamic changes in the morphology of a two-phase interface into a quantifiable representation of its stiffness. This approach underscores the imperative requirement for a meticulous and uniform quantitative delineation of the demarcation between the solid and liquid states. A precise and comprehensive understanding of the solid-liquid interface is essential in order to carry out a rigorous quantitative analysis of interfacial stiffness.

2.1 Material

Aluminiuim-copper alloys, commonly known as Al-Cu alloys, belong to a class of Aluminiuim alloys that consist predominantly of Aluminiuim (Al) with minor quantities of copper (Cu) serving as the principal alloying constituents. These alloys play a crucial role in facilitating the extensive utilization of Aluminiuim as a construction material. In its pure form, Aluminiuim exhibits a relatively low hardness, rendering it unsuitable for numerous structural applications. Nevertheless, the incorporation of alloying elements such as copper can enhance the hardness and structural suitability of Aluminiuim alloys.

Besides the inclusion of Aluminiuim-copper alloys, there exist alternative Aluminiuim alloys that possess hardening capabilities, namely aluminum-magnesium-silicon alloys (AlMgSi) and naturally hard (non-hardenable) alloys [16]. The utilization of diverse alloy formulations enables the customization of Aluminiuim for specific applications, thereby achieving the desired equilibrium between strength, durability, and other pertinent characteristics.

Alloys composed of Aluminiuim and copper are categorized within the 2000 series of alloys according to the International Alloy Designation System (IADS). The International Alloy Designation System (IADS) was initially established in 1970 by the Aluminiuim Association with the purpose of establishing a uniform method for designating and classifying various Aluminiuim alloys [16]. The alloys 2014 and 2024 hold particular significance within the 2000 series. These alloys are widely utilized in the construction of airframes, rendering them indispensable materials in the aerospace sector.

Aluminum alloys are widely recognized as highly desirable materials within the transportation industry due to their exceptional combination of properties. These alloys exhibit exceptional mechanical strength, resistance to corrosion, ease of casting, lightweight characteristics, and a minimal rate of shrinkage. These characteristics make them essential in a wide range of industries, including automotive, defense, electronics, aerospace, and engineering. Aluminum components are extensively utilized in various sectors, playing a significant role in a wide range of applications such as electric motor gaskets, armored vehicle wheels, and tank turrets [17].

In recent times, there has been a noticeable shift in the primary areas of interest within the automotive and aerospace sectors. Both industries are motivated by a steadfast pursuit of materials that not only provide decreased weight but also offer unmatched performance. Explore the domain of binary aluminum-copper alloy systems, a captivating area of research. The rationale behind this transition is rooted in the acknowledgment that the incorporation of copper into aluminum alloys offers a twofold benefit: heightened structural integrity without the undesirable repercussion of significant weight gain.

The binary Al-Cu alloys represent a distinctive alloy system that amalgamates the remarkable characteristics of aluminum and copper. These alloys possess the ability to attain significant strength while maintaining a lightweight composition. Additionally, they inherit the desirable properties of corrosion resistance and castability from cast aluminum alloys. Consequently, Al-Cu alloys find extensive utilization in diverse transportation sectors, encompassing automotive components like pistons and connecting rods, aircraft parts such as landing gear and wing spars, and marine structures including propellers and rudders.

2.2 Molecular Dynamics

Researchers use a multi-scale simulation methodology to simulate intricate material responses in computational studies, which is often a more cost-effective alternative to traditional experimental approaches. Depending on the specific objectives of the research, this comprehensive strategy encompasses a spectrum of scales ranging from the electron-level complexities of quantum mechanics to the grander dimensions of continuum mechanics. Molecular Dynamics (MD) simulations, which are routinely performed at the

nanoscale in three spatial dimensions, are an important component of this multi-scale approach. These simulations use quantum mechanics-derived force-field parameters to delineate atomic interactions, providing an invaluable tool for exploring and understanding material behaviors [13].

MD simulations have received widespread acclaim in the scientific community for their ability to probe various material attributes due to their relative simplicity and the substantial computational horsepower at their disposal. MD simulations are frequently used by researchers to investigate phenomena such as elastic behavior, grain boundary dynamics, dislocation motion, and the intricate interplay of interfaces within materials. However, the computational resources required for MD simulations are typically substantial, limiting their utility to the nano-scale. These simulations carefully track and examine the complex motions of atoms within an N-body system, operating at the extremely fine atomic scale, using a combination of fundamental concepts from classical mechanics, including Newton, Euler, Hamilton, and Lagrange mechanics [18,19].

In the context of calculating properties closely related to interface characteristics, delamination phenomena, stiffness coefficients, free energy profiles, anisotropic behaviors, and energy landscapes, this dissertation represents a noteworthy application of MD simulations. The analysis of composite materials under tensile loading conditions, the investigation of dendrite growth mechanisms, and the investigation of grain boundary behaviors in materials with different alloy concentrations are just a few of the real-world problems that these calculations are helpful in solving [13].

2.3 MD Principles

The classical equations of motion derived from Newton's second law, which states that force (f), equals mass (m) times acceleration ($\ddot{r}$), are solved using numerical techniques in Molecular Dynamics (MD) simulations. Time integration is used to accomplish this [17,18] in an N-body system, this procedure can be modified for each individual atom, i as:

$$f_i = m_i \, \ddot{r}_i \tag{2}$$

$$f_i = -\frac{\partial}{\partial r_i} U(r^N) \tag{3}$$

In this case, "U" stands for the potential energy and " $r^N = (r_1, \, r_2, \, r_3, \, r_N)$" for the vector that contains all of the coordinates for the 3N atoms. Numerical simulations enable the computation of the paths taken by each particle in the system given the initial position and velocity conditions. Since there are more equations of motion in MD simulations than there are degrees of freedom, there are significant computational requirements. Numerical algorithms designed to lessen the strain on computing resources are incorporated into programs like LAMMPS to ease this computational burden. However, it is wise to start by introducing Lagrangian mechanics in order to gain a thorough understanding of the topic.

The formulation of an energy equation within a generalized coordinate system that was selected at random gives rise to classical Lagrangian mechanics. In this context, the contrast between kinetic energy, denoted as 'K,' and potential energy is established as the Lagrangian equation.

$$\mathcal{L}(q_S) = K - U \tag{4}$$

To solve the equations of motion, we perform a second-order partial derivative in the generalized coordinate system with respect to both position and velocity. This coordinate system, denoted as $q = q_1, q_2, q_3, \dots, q_s$, is defined by the smallest number of independent parameters, denoted as s, that are required to describe the system's state. Each particle in the systems under consideration in this study has two independent Cartesian coordinates. $\dot{q}$ and $\ddot{q}$ represent the velocity and acceleration of these components, respectively. Following classical mechanics principles, the total kinetic energy of the entire system is defined as the sum of individual particle contributions, with an assumed constant mass, m:

$$K(\dot{q}_S) = \sum_{n=1}^{N} 0.5m(v_n^2) \tag{5}$$

$$v_n = \sqrt{\dot{q}_i^2 + \dot{q}_j^2} \tag{6}$$

The potential energy of the system is calculated by adding the individual particle potential components, denoted as u_n. These components are typically defined as a function of the distance between two points, r, and include both attractive and repulsive properties. The system's forces are derived from the rate of change (derivative) of potential energy with respect to the separation distance. When a single particle exists within a constrained environment, it is referred to as a single-body potential, indicating that the system is influenced by only one potential energy component:

$$U = \sum u_n(r) \tag{7}$$

$$f = -\frac{dU}{\partial r} \tag{8}$$

The Lagrangian equation of motion can be written as follows with the kinetic and potentials defined as functions of position, q, and velocity, $\dot{q}$:

$$\frac{d}{dt}\frac{\partial L}{\partial \dot{q}_a} - \frac{\partial L}{\partial q_a} = 0 \quad , a = 1, 2, 3, \dots, s \tag{9}$$

As a result, in a Lagrangian system, the number of equations of motion corresponds to the number of independent parameters or degrees of freedom (DOFs). Hamiltonian mechanics, which calculates the energy of a generalized coordinate system in the same way, provides an alternative method and expresses the equation using momentum, denoted as, p, which can be written in relation to the Lagrangian:

$$H = \sum p_a q_a - \mathcal{L} \tag{10}$$

With the equations of motion:

$$\dot{q}_a = \frac{\partial H}{\partial p_a} \tag{11}$$

$$\dot{p}_a = -\frac{\partial H}{\partial q_a} \tag{12}$$

The equations of motion in both Lagrangian and Hamiltonian mechanics are solved numerically using numerical integrators and an initial position and velocity vector as input [13].

The Verlet algorithm is the most fundamental and widely used integration technique [17,18]. This method commonly calculates atom positions at specific time steps,

such as "$t, t - \delta t$," and "$t + \delta t$." However, it is important to note that velocity and acceleration cannot be directly computed using this method; instead, they are inferred using trajectory equations, which necessitate additional computational steps. The Velocity Verlet [20,21] algorithm, a modified version of this algorithm, has been adopted in computational software packages such as LAMMPS [21]. It can be used to calculate positions, velocities, and accelerations at a given time, "$t + \delta t$":

$$r(t + \delta t) = r(t) + v(t)\delta t + \frac{1}{2}a(t)\delta t^2 \tag{13}$$

$$v\left(t + \frac{1}{2}\delta t\right) = v(t) + \frac{1}{2}a(t)\delta t \tag{14}$$

$$v(t + \delta t) = v\left(t + \frac{1}{2}\delta t\right) + \frac{1}{2}a(t + \delta t)\delta t \tag{15}$$

The ability to compute velocity and position at a specific time step illustrates the effectiveness and precision of the Velocity Verlet algorithm. As a result, this method provides a solid methodology while reducing the need for extensive data storage and improving computational memory utilization.

2.4 CFM (Capillary Fluctuation Method)

CFM, a statistical mechanics-based technique, connects interfacial stiffness to the motion of atoms in a two-phase interface [23,12,25]. It has been applied to a variety of materials and has been demonstrated to be connected to weakly anisotropic material free energy and anisotropy parameters. These CFM-derived properties are applied across scales and contrasted with experimental results. There hasn't been any published research on the

variables that affect stiffness, free energy, and anisotropy results, particularly when it comes to precisely defining the fluctuating interface height using order parameters and fractal dimensions.

By addressing these issues in aluminum and copper solid-liquid interfaces, this study aims to broaden the application of CFM. Due to complex interactions, it is difficult to study the atomic-scale interface between solid and liquid phases, especially using the capillary fluctuation method (CFM) to calculate characteristics like stiffness, anisotropy, and free energy [22-24]. There is a dearth of documentation for CFM's practical use, including interface fractal dimension definitions, despite the fact that it has been used for crystalline structures and some applications involving water and ice.

The capillary fluctuation method (CFM) on a thin quasi-2D setup is frequently used to determine the interfacial stiffness in equilibrium solid-liquid solidification systems. This method establishes a relationship between interfacial stiffness and the average square amplitude, written as $h(x) = \Sigma_k A(k)e^{ikx}$, using equipartition and Fourier mode analysis,

$$\langle |A(k)|^2 \rangle = \frac{k_b T_\sigma}{bW(S(\theta))k^2} \tag{16}$$

Boltzmann constant is denoted here by k_b the system's temperature by T_σ its width by W its thickness by b the wavenumber by k, the interface's free energy by γ and the angle between the interface's normal and the nominally flat normal direction by θ. The interfacial stiffness, which we define as $S(\theta) = \gamma + \gamma_{\theta\theta}$ implicitly assumes that the interface is in equilibrium, much like the Gibbs-Thomson condition. To incorporate a temperature-dependent term into the capillary fluctuation method (CFM), we must first investigate how

19

the system's energy is derived and how it relates to temperature-dependent aspects of the interface and material properties. This is critical for understanding how temperature affects the behavior of the solid-liquid interface [13].

Hoyt proposed an equation to represent the surplus free energy of a balanced two-phase system as $E = b \int_0^w \gamma(\theta) \, ds$ [24]. Upon closer examination at the atomic level and within brief time intervals, it is observed that the fluctuations occurring at the interface exhibit relatively small amplitudes. These fluctuations can be described by the mathematical expressions $\sqrt{1 + h'(x)^2} = 1 + \frac{h'(x)^2}{2}$ and $h'(x) = tan(\theta) \approx \theta$. The inclusion of the temperature gradient, represented as G, enables us to reevaluate the energy equation, which can be expressed as:

$$E = b \int_0^w \gamma(\theta, G)\sqrt{1 + h'(x)^2} \, dx \tag{17}$$

In order to account for the influence of a temperature gradient in one dimension, denoted as $G = \nabla T = \frac{dT}{dh}$ on the interfacial free energy, γ ,we modify Hoyt's approach by expanding the expression with multiple variables using a second-order Taylor series. The equation can be expressed as:

$$\gamma_{(\theta, G)} \approx \gamma + \gamma_\theta \theta + \gamma_G G + \frac{1}{2}(\gamma_{\theta\theta}\theta^2 + \gamma_{GG}G^2) + \gamma_{\theta G}\theta G \tag{18}$$

By substituting Equation (16) into Equation (17), the energy equation can be decomposed into the summation of five distinct contributions along the interface, as delineated in Table 1.

Table 1: Approximate energy contribuation at an interface with applied temprature gradient

E:	$$b \int_0^{} \gamma(\theta, G)\sqrt{1 + h'(x)^2}\, dx = \sum_{i=1}^{5} E_i$$
E₁:	$$b \int_0^{w} \left[\gamma + \gamma_G + \frac{\gamma_{GG} G^2}{2} \right] dx$$
E₂:	$$b \int_0^{w} h'(x)[\gamma_0 + \gamma_{\theta G} G]\, dx = 0$$
E₃:	$$b \int_0^{w} h'(x)^2 \left[\frac{\gamma}{2} + \frac{\gamma_{\theta\theta}}{2} + \frac{\gamma_G G}{2} + \frac{\gamma_{GG} G^2}{4} \right] dx$$
E₄:	$$b \int_0^{w} h'(x)^3 \left[\frac{\gamma_\theta}{2} + \frac{\gamma_{\theta G} G}{2} \right] dx = 0$$
E₅:	$$b \int_0^{w} h'(x)^4 \left[\frac{\gamma_{\theta\theta}}{4} \right] dx = 0$$

When considering periodic boundary conditions parallel to the interface length, it is possible to eliminate the second contribution term, $\int_0^{w} h'(x)\, d(x) = 0$." In a similar vein, under the assumption of minor variations in height, the inclusion of higher-order terms in the equation $h'(x) \approx 0$ results in the exclusion of the fourth and fifth energy contributions. The equation can be further simplified by regarding the initial contribution as the energy associated with a planar interface and introducing the notation $\Delta E = E - E_1$

$$\Delta E = \frac{1}{2} b \left(\gamma + \gamma_{\theta\theta} + \gamma_G G + \frac{\gamma_{GG} G^2}{2} \right) \int_0^w h'(x)^2 \, dx \tag{19}$$

When Equation (19) is compared to Hoyt's equilibrium system derivation [24], $\Delta E = \frac{1}{2} b (\gamma + \gamma_{\theta\theta}) \int_0^w h'(x)^2 \, dx$ it can be observed that the equations are identical under the condition of zero gradient. The term within the parenthesis can be used to define stiffness.

$$S_{(\theta,G)} = \gamma + \frac{1}{2} \gamma_{GG} G^2 + \gamma_{\theta\theta} + \gamma_G G \tag{20}$$

The utilization of the second-order expansion of the Taylor series for interfacial free energy leads to the emergence of an initial hypothesis, indicating a power relationship between stiffness and the gradient. The potential variability of this relationship across different materials has not been investigated in the present study. The recently obtained stiffness is consistent with the boundary conditions for achieving equilibrium in the absence of a thermal gradient, specifically expressed as $S_{(\theta,G)} = \gamma + \gamma_{\theta\theta}$. By incorporating the gradient-based interfacial stiffness into Equation (16), we can derive an approximation of a CFM equation that takes into account an applied temperature gradient.

$$\langle |A(k)|^2 \rangle = \frac{k_b T_\sigma}{bW \left(\gamma + \gamma_{\theta\theta} + \gamma_G G + \frac{\gamma_{GG} G^2}{2} \right) k^2} \tag{21}$$

However, it should be noted that this derivation makes the assumption that variations in height are exclusively caused by alterations in interfacial stiffness. This oversimplification of the dynamics in rapid solidification systems should be taken into consideration. The research conducted by Karma on the phenomenon of fluctuations in

solidification [25] reveals the existence of supplementary factors influencing these fluctuations, which are not contingent upon the material's stiffness. The derivation of a fluctuation spectrum equation for a stationary interface in a temperature gradient served as an illustration of this phenomenon.

$$\langle \xi_k \xi_{-k} \rangle_G = \frac{k_b T_\sigma}{\gamma(k^2 + a^{-2})} \tag{22}$$

where $\langle \xi_k \xi_{-k} \rangle_G$ represents the fluctuation spectrum of a symmetric structure experiencing a temperature gradient. Additionally, $a = \sqrt{\frac{rT_\sigma}{LG}}$ where L denotes the latent heat per unit volume. By utilizing the quasi-two-dimensional formulation of Equations (20) and (21), it is possible to deduce an equation that can be solved for the gradient-dependent stiffness term.

$$\langle |A(k)|^2 \rangle = \frac{k_b T_\sigma}{bW S_{(\theta,G)}(k^2 + a^{-2})} \tag{23}$$

represents the average squared magnitude of the wavevector a in relation to the surface energy denoted by γ under equilibrium conditions. The determination of stiffness can be achieved by creating a plot of the variable $\frac{k_b T_\sigma}{bW \langle |A(k)|^2 \rangle}$ against (k^2) and analysing the linear slope for low wavenumber values.

2.5 Anisotropy

Hoyt et al. (23) conducted a study in which they established that the interfacial free energy of solid-liquid interfaces exhibiting limited anisotropy in their crystalline structure

can be mathematically described as a function of the interface normal, denoted as $(\hat{n})$. The present expression can be extended through the utilization of cubic harmonics, as documented in references [22, 26,27], yielding the following representation:

$$\frac{\gamma(\hat{n})}{\gamma_0} = 1 + e\left(\sum_{i=1}^{3} ni^4 - \frac{3}{5}\right) + d\left(3\sum_{i=}^{3} n_i^6 + 66n_1^2 n_2^2 n_j^2 - \frac{17}{7}\right) \tag{24}$$

The symbol n_j is used to denote the components of the interface normal $\hat{n}$ in the Cartesian coordinate system (x_1, x_2, x_3). The parameters denoted as e and d are associated with the surface anisotropy properties. In the context of quasi-2D structures, wherein the thickness is deemed insignificant, the interface normal can be delineated as:

$$n_i = [sin(\theta)\hat{x}_1 + cos(\theta)\hat{x}_3]\hat{z}_{i_x} \quad i = 1,2,3 \tag{25}$$

$$\hat{x}_1 = \frac{a_i\hat{z}_1 + b_i\hat{z}_2 + c_i\hat{z}_3}{\sqrt{a_i^2 + b_i^2 + c_i^2}} \tag{26}$$

The symbol $\hat{z}_1$ denotes the unit vectors [100], [010], and [001]. The parameters a_i, b_i, c_i are utilized to denote the orientation of the interface. Under the assumption that the anisotropic properties of the interface between a solid and a liquid remain unchanged under thermal conditions, it is feasible to develop mathematical equations that describe various equilibrium orientations that meet the condition $\gamma + \gamma_{\theta\theta|\theta=0}$ as outlined in Table 2. Within the confines of a theoretical framework, it is possible to calculate the interfacial energy, along with the anisotropic parameters denoted as $\in$ and δ through the examination of a collection comprising three distinct orientations. To ensure the precision of these

calculations, a thorough analysis is performed on a total of eight interface orientations. In this subsequent section, we examine the material characteristics of the interface between solid and liquid Al-Cu alloy in the context of thermal non-equilibrium. Additionally, we establish a discernible pattern that can be employed for the purpose of interpolation. Our investigation not only assesses the interfacial stiffness and energy but also examines the hypothesis that the anisotropy parameters, referred to as *e* and *d* remain independent variables in relation to the applied gradient [13].

Table 2: Anisotropy for Multiple interface orientations

ORIENTATION	$\gamma+\gamma''/\gamma0$
100[010]	1-3.6e-11.4d
110[001]	1+3.9e+11.1d
110[1-10]	1-2.1e+26.1d
110[-110]	1-2.1e+26.1d
111[1-10]	1-2.4e-20.3d
111[-1-12]	1+9e-9.4d
120[001]	1+1.2e+3d
120[2-10]	1-2.64e+12.6d

The first number of the notation indicates the direction perpendicular to the interface, the number in brackets denotes the direction along the interface length.

Chapter Three

Simulation Methodology

In this section, we describe the various Molecular Dynamics (MD) parameters and methods that we used in our study to evaluate the characteristics of the interface. This includes describing the parameters of our simulation model, explaining the strategy used to produce a dual-phase state, looking at the use of thermal gradients, and outlining the steps for determining the boundary between the solid and liquid phases.

3.1 Simulation Structure

Use of the LAMMPS molecular dynamics software is required to calculate the interfacial free energy of AL-CU alloy [28]. Depending on their lattice orientations, the Aluminiuim specimens used in the MD simulations have different configurations. However, each structure follows the CFM assumptions, where $b << W$ and the height of the structures is determined to be twice their width, denoted as $H = 2W$ in order to reduce interactions between adjacent interfaces and boundaries, as shown in Figure 3. As a result, variations are present in the dimensions and atom counts for each interface orientation, as shown in Table 3.

Table 3: Simulation size of eight interface orientations

ORIENTATION	ATOMS	H(A)	W(A)	B(A)
100[010]	207360	248.811	295.409	49.2453
110[001]	414720	353.137	295.29	69.5754
110[1-10]	414720	353.195	417.452	49.208
110[-110]	414720	352.017	417.842	49.2584
111[1-10]	829440	433.46	417.331	80.3137
111[-1-12]	829440	431.689	482.6	69.6514
120[001]	373248	333.914	296.014	66.1524
120[2-10]	373248	334.023	396.493	49.2694
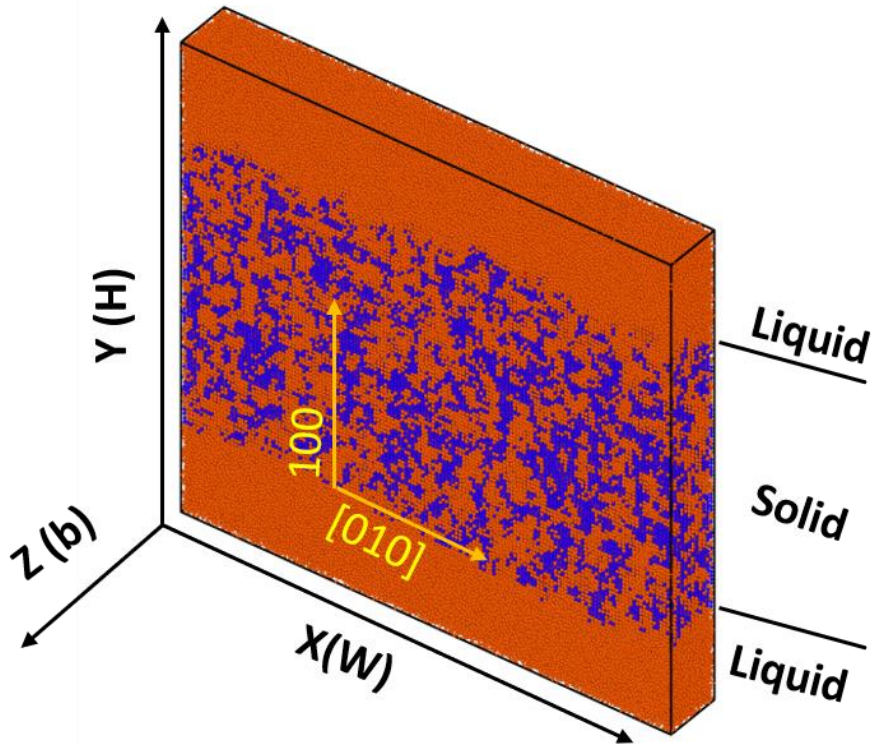
Figure 3: Quasi-2D model of 100[010] orientation of solid-liquid simulation model for Al-Cu alloy

We have used an embedded-atom method (EAM) potential [29] that has been designed specifically for AlCu alloys in the context of our research. We predict that in these hypothetical calculations, the concentration of alloyed elements within the material may have an impact on the free energy calculations in addition to the gradient. It is important to note the differences between our chosen EAM potential and some of the more recent potentials created by Mendelev and colleagues [30], which were primarily intended for the isolated applications of either aluminum or copper. Contrarily, the EAM potential we've used here is specifically designed for alloys, taking into account situations in which different elements coexist in the same material. It's crucial to remember that the alloy-based EAM potential we chose wasn't specifically tailored for extremely high temperatures. We took this into account and performed our calculations at three different temperatures: 905K, 888K, and 874K. These temperatures were chosen in recognition of the potential limitations of the EAM potential at higher temperature regimes, which were selected to be to be inside solid-liquid miscibility gap [31]. We aimed to obtain accurate and significant results while remaining within the applicability of the potential by running simulations at these lower temperatures.

3.2 Solid- Liquid phase structure

Numerous methods exist for creating a Molecular Dynamics (MD) model that simulates a two-phase solid-liquid system. A multi-step process was used in this study to ensure an accurate representation of such a system under thermal equilibrium conditions.

The NVE ensemble is used first to equilibrate the model to the predicted melting temperature while applying a fixed Berendsen barostat to maintain a zero external pressure

state. A full-structure Langevin thermostat set to the approximate melting temperature regulates the temperature parameter. The structure is allowed to stabilize during a 20ps equilibration phase carried out with a 2fs time step. The liquid portion of the structure then defines a new thermostat. Over the course of 50 ps, the temperature is raised, and it is then gradually lowered to the melting point. The full-structure thermostat keeps the temperature constant throughout this process until equilibrium is reached, which in our simulations takes about 1 nanosecond (ns).

It is important to pay close attention to the solid-liquid interface during this equilibration phase to make sure there is no translational movement and to confirm the accuracy of the presumptive melting temperature. The Langevin thermostat is turned off once the melting temperature has been confirmed and the system has reached equilibrium.

The pressure barostat is then removed, leaving the system in the NVE ensemble for an additional 200 ps of further equilibration using only the Berendsen barostat. Under thermal equilibrium conditions, this meticulous process produces a stable solid-liquid interface, as shown in Figure 4. The objective of this methodology is to provide a trustworthy representation of a solid-liquid interface in MD simulations while being applicable for general material selection purposes. [13]
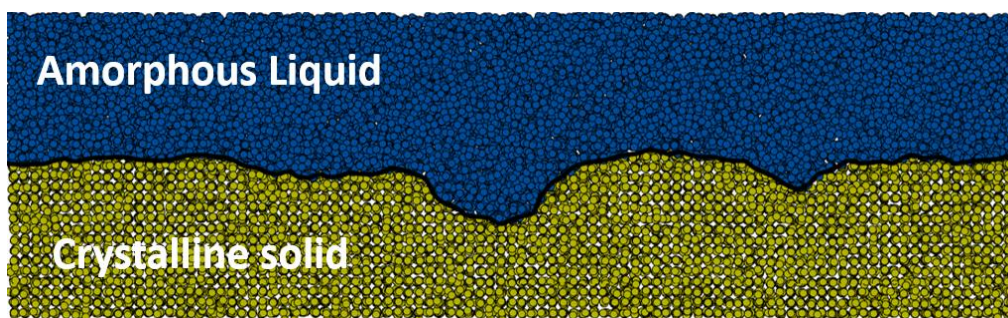
Figure 4: Atomic Structure of a system in two-phase state consisting of an amorphous liquid and crystalline solid. Interface graphically defined as the boundary between the two phases.

3.3 Application of Thermal Gradients

Now that we have a stable two-phase structure in thermal equilibrium at the melting temperature, we describe a method to introduce thermal gradients while maintaining the interface's stationary state. The selected approach for this investigation involves the utilization of a Langevin thermostat with a thickness of 20 angstroms, positioned at the center of each phase. The remaining regions of the model are subjected to an NVE ensemble, as depicted in Figure 5.

These thermostats, being dynamic regions, allow for unrestricted atomic motion to enter and exit the system. In order to mitigate any potential negative impact on the interface, the dimensions of these thermostats have intentionally been limited to a compact region within the model. The efficacy of this precaution is confirmed by the temperature profile obtained after the equilibration procedure. [13]

The Langevin thermostats are subsequently and gradually modified over a time period of 200ps in order to attain the target temperatures, while simultaneously upholding the boundary condition of zero external pressure. In order to establish the new temperature profile, the simulation undergoes an additional 200ps of equilibration. Subsequently, the

simulation is extended by an additional duration of 400ps wherein snapshots of the atomic positions are captured at regular intervals of 0.2 ps. Consequently, a grand total of 1,000 images have been acquired depicting the atomic structure, which are subsequently employed for the application of the CFM. The comprehensive methodology employed allows for the establishment and preservation of thermal gradients within the system, while simultaneously ensuring a stable and precisely regulated solid-liquid interface.

Temperatures in the solid and the liquid were set to comply with the prescribed gradients and the values are shown in the able 4,5 and 6. Table shows mean temperature of the system. Term used for CFM calculation of interface properties.

Table 4: Temperature gradient for 905 and thermostat definition

Orientation	Gradient (K/nm)	Temperature (K) (Liquid)	Temperature (K) (Solid)
110[010]	12	978.837	831.163
	24	1052.67	757.326
	36	1126.51	683.488
110[001]	12	1009.89	800.108
	24	1114.78	695.217
	36	1219.68	590.325
110[1-10]	12	1010.88	799.116
	24	1116.77	693.231
	36	1222.65	587.347
110[-110]	12	1009.8	800.205
	24	1114.59	695.41
	36	1219.39	590.615
111[1-10]	12	1033.68	776.316
	24	1162.37	647.632
	36	1291.05	518.949
111[-1-12]	12	1033.69	776.313
	24	1162.37	647.625
	36	1291.06	518.938
120[001]	12	1003.44	806.558
	24	1101.88	708.117
	36	1200.33	609.675
120[2-10]	12	1004.43	805.574
	24	1103.85	689.147
	36	1203.28	606.721

Table 5 Temperature gradient for 888 and thermostat definition

Orientation	Gradient (K/nm)	Temperature (K) (Liquid)	Temperature (K) (Solid)
110[010]	12	961.837	814.163
	24	1035.67	740.326
	36	1109.51	666.488
110[001]	12	992.89	783.108
	24	1097.78	678.217
	36	1202.68	573.325
110[1-10]	12	993.88	782.116
	24	1099.77	676.231
	36	1205.65	570.347
110[-110]	12	992.8	783.205
	24	1097.59	678.41
	36	1202.39	573.615
111[1-10]	12	1016.68	759.316
	24	1145.37	630.632
	36	1274.05	501.949
111[-1-12]	12	1016.69	759.313
	24	1145.37	630.625
	36	1274.06	501.938
120[001]	12	986.44	789.558
	24	1084.88	691.117
	36	1183.33	592.675
120[2-10]	12	987.43	788.574
	24	1086.85	672.147
	36	1186.28	589.721

Table 6: Temperature gradient for 874 and thermostat definition

Orientation	Gradient (K/nm)	Temperature (K) (Liquid)	Temperature (K) (Solid)
110[010]	12	947.837	800.163
	24	1021.67	726.326
	36	1095.51	652.488
110[001]	12	978.89	769.108
	24	1083.78	664.217
	36	1188.68	559.325
110[1-10]	12	979.88	768.116
	24	1085.77	662.231
	36	1191.65	556.347
110[-110]	12	978.8	769.205
	24	1083.59	664.41
	36	1188.39	559.615
111[1-10]	12	1002.68	745.316
	24	1131.37	616.632
	36	1260.05	487.949
111[-1-12]	12	1002.69	745.313
	24	1131.37	616.625
	36	1260.06	487.938
120[001]	12	972.44	775.558
	24	1070.88	677.117
	36	1169.33	578.675
120[2-10]	12	973.43	774.574
	24	1072.85	658.147
	36	1172.28	575.721

As depicted in Figure 5, the introduction of a temperature gradient to a system with a non-uniform material composition for both phases results in the manifestation of a non-linear thermal conductivity, which is represented as $k(T)$.
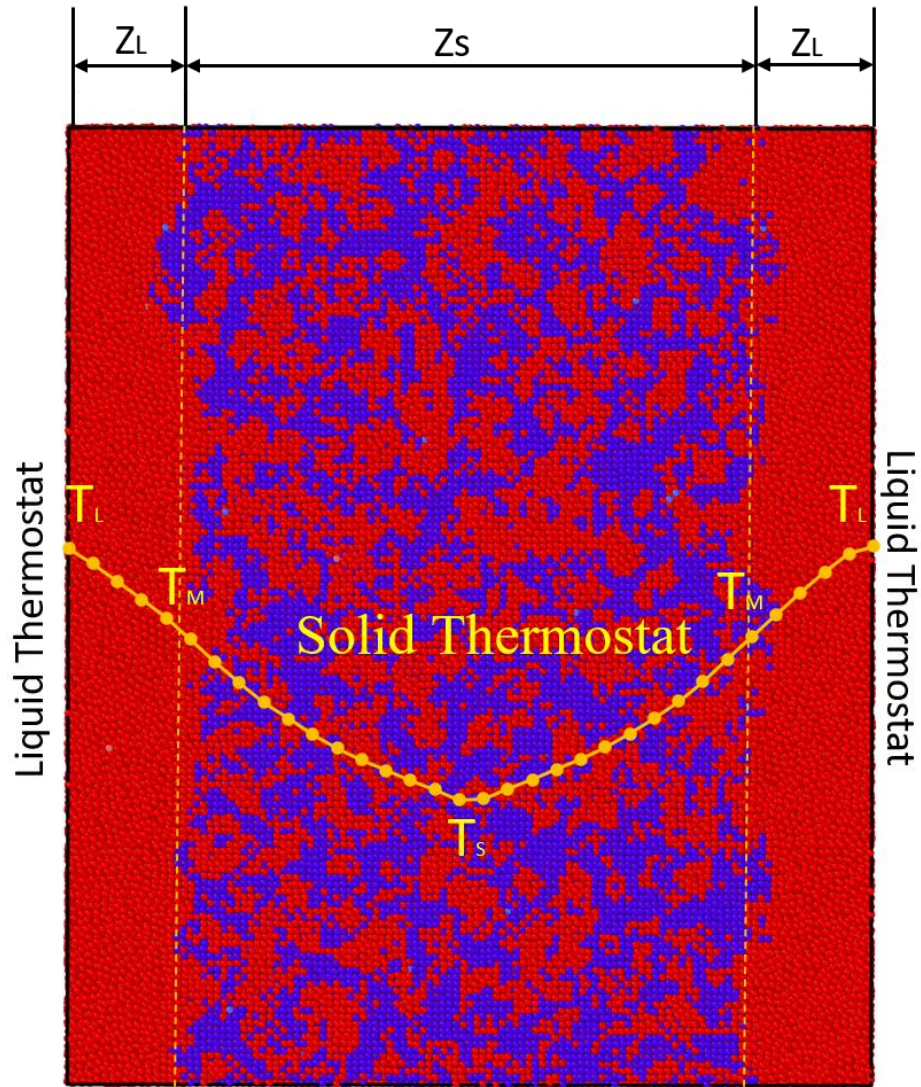
Figure 5: Applied thermostat to a solid-liquid structure of Al-Cu alloy

3.4 Defining the Solid-liquid interface

We use a centrosymmetry parameter for FCC (Face-Centered Cubic) structures, denoted as $p = \sum_{i=1}^{6} |\vec{r}_i + \vec{r}_{i+6}|^2$, to pinpoint the exact location of the interface. Each atom is given this parameter, denoted by the letter i and r stands for the vector position of the closest neighbors. We create a mesh out of each structure and collect the mean centrosymmetry parameter in predetermined bins for the duration of the simulation. The extent to which the interface is characterized depends heavily on the size of these bins along the x-axis. We have established a bin size of 2.0850 x 2.0850 A^2 for this study, to ensure consistency across various model sizes. After computing the average centrosymmetry parameter, we build height profiles perpendicular to the interface and then present the results as mean centrosymmetry parameters for each bin, as shown in "Figure 6" The point where the centrosymmetry shows the greatest difference between the region above and below the specified height point is where we define the interface. This procedure is repeated along the entire length of the interface to produce an interface height profile for each snapshot, which is denoted by the symbol, *h(x)*, The application of the CFM then makes use of these profiles. [35]
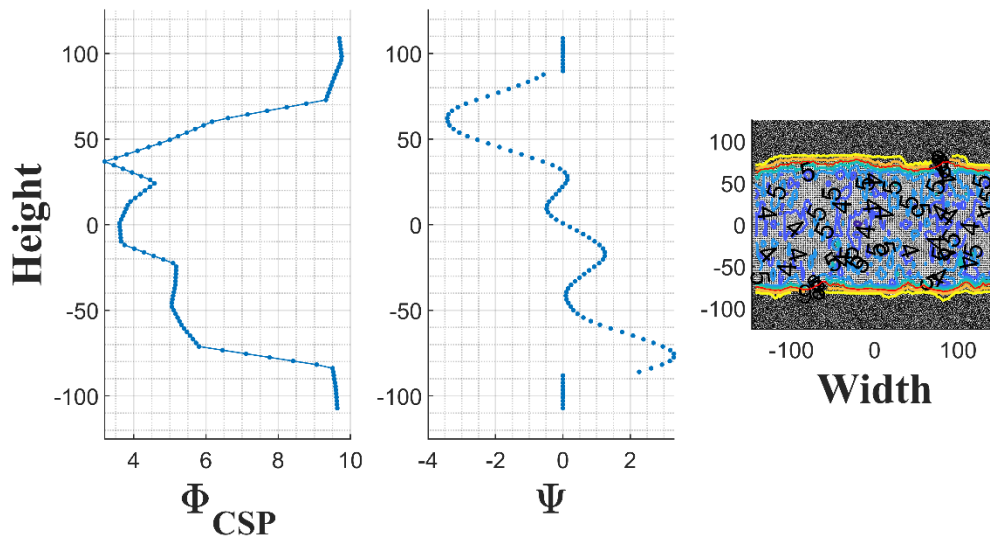
Figure 6: Solid- Liquid interface of Al-Cu defined using CSP and maxium difference function. Contours shows 2D distribuation of order parameter.

Chapter Four

4.1 Result

This study aims to examine the impact of different levels of copper content on both the interfacial energy and its anisotropy in Al-Cu alloys. The alloys being examined consist of copper concentrations of 2%, 3.58%, and 5.065% is presented in Figure 7. These alloys are subjected to temperatures of 905K, 888K, and 874K, respectively.

Table 7: Temprature and Cu % (Atomic)

Case	*Temperature*	*Cu %*
1	905	2
2	888	3.58
3	874	5.065

The alloys under investigation are examined in a variety of eight distinct interface orientations, which are comprehensively described in Table 3. The solidification process is initiated by extracting thermal energy from the lower region of two-dimensional domains. In order to gain a comprehensive understanding of the effects of different concentrations of copper, we utilize molecular dynamics (MD) coupled with Monte Carlo (MC) simulations to investigate the interfacial energy and its anisotropy. This methodology enables the investigation of the impacts of varying copper concentrations on the behavior of the material.
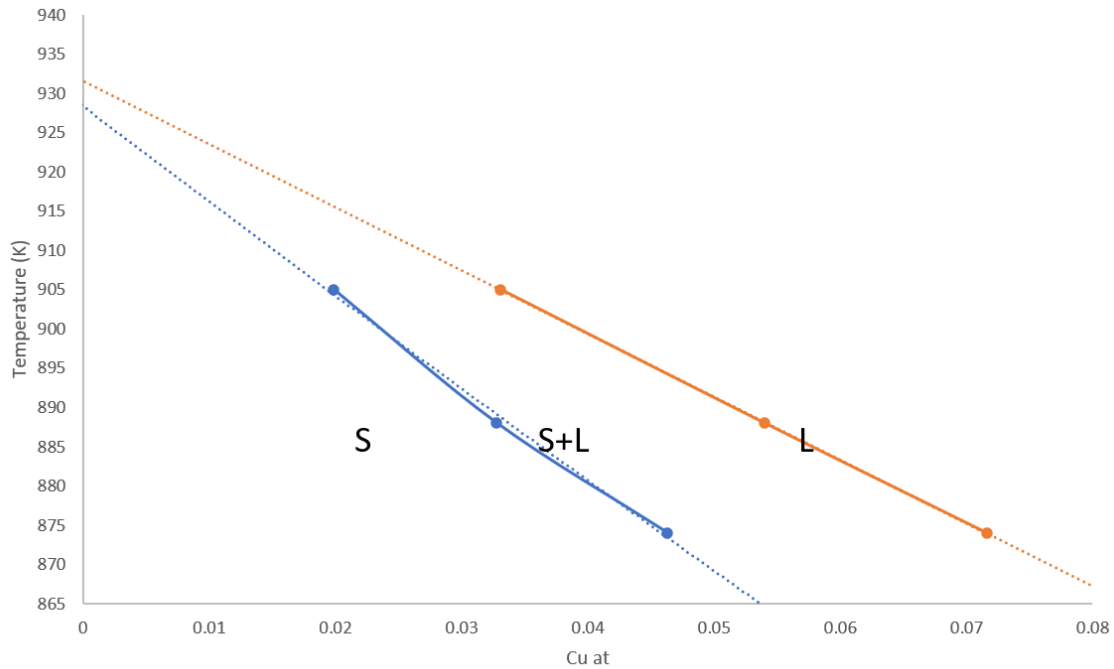
Figure 7: Al-rich composition-temprature phase diagram for AL-Cu alloy calculaed by MD simulations and Thermo-Cal. The symbols L and S denote the liquid and solid (S-L) phase, respectively

The primary objective is to investigate the anisotropic characteristics of the material, which exert a substantial influence on its behavior at the interface between the solid and liquid phases. In order to accomplish this objective, we undertake a multifaceted procedure. In the first stage, we perform molecular dynamics (MD) simulations at the melting temperature, employing a solid-liquid system. In Metropolis MC we swap atom using Boltzmann probability to accept or reject the exchange. This algorithm takes system to equilibrium. Subsequently, we proceed to conduct simulations incorporating approximate temperature gradients of 0, 12, 24, and 36 K/nm. These simulations enable us to analyze the properties of Solid-liquid interface for different temperature gradients.

39

Our main goal is to establish a correlation between interfacial energy and the gradient of temperature. The present study systematically investigates and validates the relationship in question, in accordance with the theoretical framework outlined above. The verification process provides valuable insights into the relationship between interfacial energy and variations in the magnitude of temperature gradient.

Moreover, we aim to examine the hypothesis that the presence of temperature gradient does not alter the material anisotropy. In order to substantiate this hypothesis, we employ a calculation method to determine the interfacial energy. This calculation involves utilizing both equilibrium anisotropy parameters, as well as parameters that are customized to account for the specific temperature gradient in question. This comparative analysis facilitates the identification of potential variations in the anisotropic behavior of materials under different gradient conditions.

Our stiffness calculations enable us to determine the interfacial free energy and anisotropy parameters. We have three unknows, namely the interface free energy γ_0, and two anisotropic parameters, e and d. The data for the stiffness that we have obtained for eight different orientations provide eight equations and hence the problem is overdetermined as shown in table A.1. To obtain the values we pick the equations provided by three particular orientations, namely "100[010], 110[1-10], and 120[001], which results in the minimum error, Table 8 shows calculation for 905K. The derived values for these parameters are can be seen in Table 9-11 for respective temperature. It is of significance to acknowledge that the anticipated interfacial energy for Al-Cu, as determined through empirical observations and accurately calibrated EAM and MEAM potentials, lies within

the interval of "140~170 mJ/m^2" [32]. The observed discrepancy in melting temperatures among the chosen potentials can account for the relatively inadequate depiction of interfacial energy at equilibrium. This highlights the importance of employing controlled simulations as reference benchmarks in molecular dynamics (MD) investigations.

0K/NM

ORIENTATION	Case	e	d	$\gamma 0^{-1}$	result		Error	
100[010]	1	3.6	11.42857143	55	1	e	-4.92%	-0.0492421
110[1-10]	3	2.1	-26.1	50	1	d	-0.07%	-0.0007332
120[001]	8	-1.2	-2.971428571	43	1	$\gamma 0^{-1}$	0.0218	0.02175506
						$\gamma 0$	46.0	45.966316

12K/nm

ORIENTATION	Case	e	d	$\gamma 0^{-1}$	result				
100[010]	1	3.6	11.42857143	76	1	e	-5.82%	-0.0581863	18%
110[1-10]	3	2.1	-26.1	52	1	d	-0.86%	-0.0086009	1073%
120[001]	8	-1.2	-2.971428571	52	1	$\gamma 0^{-1}$	0.0173	0.01728022	
						$\gamma 0$	57.9	57.8696399	26%

24K/nm

ORIENTATION	Case	e	d	$\gamma 0^{-1}$	result				
100[010]	1	3.6	11.42857143	69	1	e	-6.44%	-0.0644133	31%
110[1-10]	3	2.1	-26.1	67	1	d	0.15%	0.00151824	-307%
120[001]	8	-1.2	-2.971428571	53	1	$\gamma 0^{-1}$	0.0175	0.01754097	
						$\gamma 0$	57.0	57.0094053	24%

36K/nm

ORIENTATION	Case	e	d	$\gamma 0^{-1}$	result				
100[010]	1	3.6	11.42857143	77	1	e	-5.60%	-0.0559607	14%
110[1-10]	3	2.1	-26.1	89	1	d	0.70%	0.00696671	-1050%
120[001]	8	-1.2	-2.971428571	65	1	$\gamma 0^{-1}$	0.0146	0.01463395	
						$\gamma 0$	68.3	68.3342409	49%

Table 8: Stiffness calculation for 0, 12, 24, 36 thermal gradient at 905K

Table 9: The average Free energy and anisotorpy parameters for Al-Cu binary system at 905 K and Thermal gradients

Gradient	e	d	γ_0
0.0	-0.0492421	-0.0007332	45.966316
12.0	-0.0581863	-0.0086009	59.2838389
24.0	-0.0644133	0.00151824	71.9878997
36.0	-0.0559607	0.00696671	84.616395

Table 10: The average Free energy and anisotorpy parameters for Al-Cu binary system at 888 K and Thermal gradients

Gradient	e	d	γ_0
0.0	-0.0632509	-0.0023218	37.7998335
12.0	-0.0565017	-0.0023243	53.8121108
24.0	-0.0530478	-0.0050078	58.1303206
36.0	-0.0627035	-0.0026994	60.0653722

Table 11: The average Free energy and anisotorpy parameters for Al-Cu binary system at 874 K and Thermal gradients

Gradient	e	d	γ_0
0.0	-0.2282364	0.0075575	18.7289706
12.0	-0.1273601	0.0031025	33.7237083
24.0	-0.2098398	-0.0136543	38.6390878
36.0	-0.1547292	-0.0125313	41.179428

After conducting verification on these parameters in three additional orientations, it is evident that the stiffness can be predicted with a margin of error from the calculated

values. The observed variation falls within the expected range for the CFM method, especially when using a few random seed numbers.

In addition, our analysis is expanded to include various temperature gradients and orientations, emphasizing the 100[010], 111[1-10] and 111[-1-12] orientations, as depicted in Figure 8. The simulations provide valuable insights into the properties of the interface that are dependent on temperature. It is important to highlight that in instances where $G=0$, the x-intercept should be located at "a^{-2}," instead of zero, as observed in the conventional equilibrium.
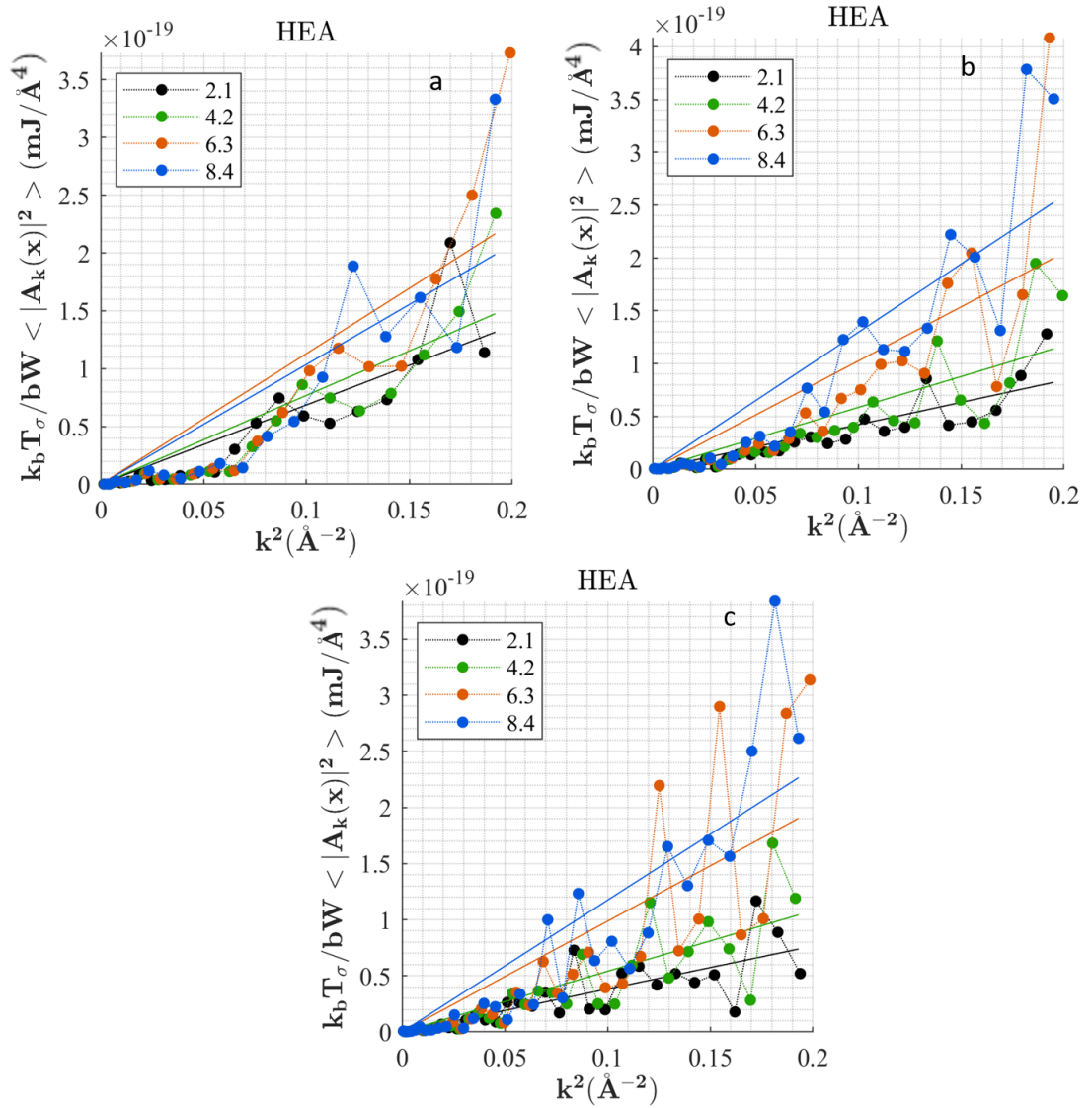
Figure 8: CFM for Al-Cu solid-liquid interface, plots of to k_B $T_m/bW\langle|A(k)/2\rangle$ versus k2 to calculated interfacial stiffness at equiibrium and temperature gradients. (a) 100[010] (b) 111[1-10] (c) 111[-1-12]
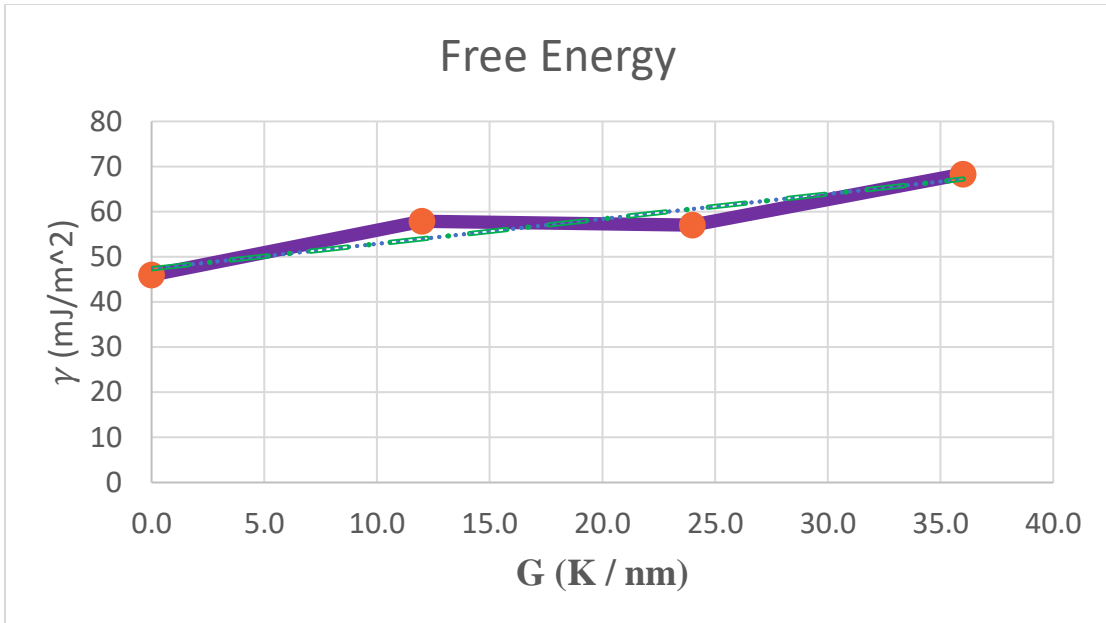
Figure 9: Temprature gradient(K) vs Free engergy (γ (mJ/m^2)) for Al-Cu alloy at Temprature 905 and Cu 2%
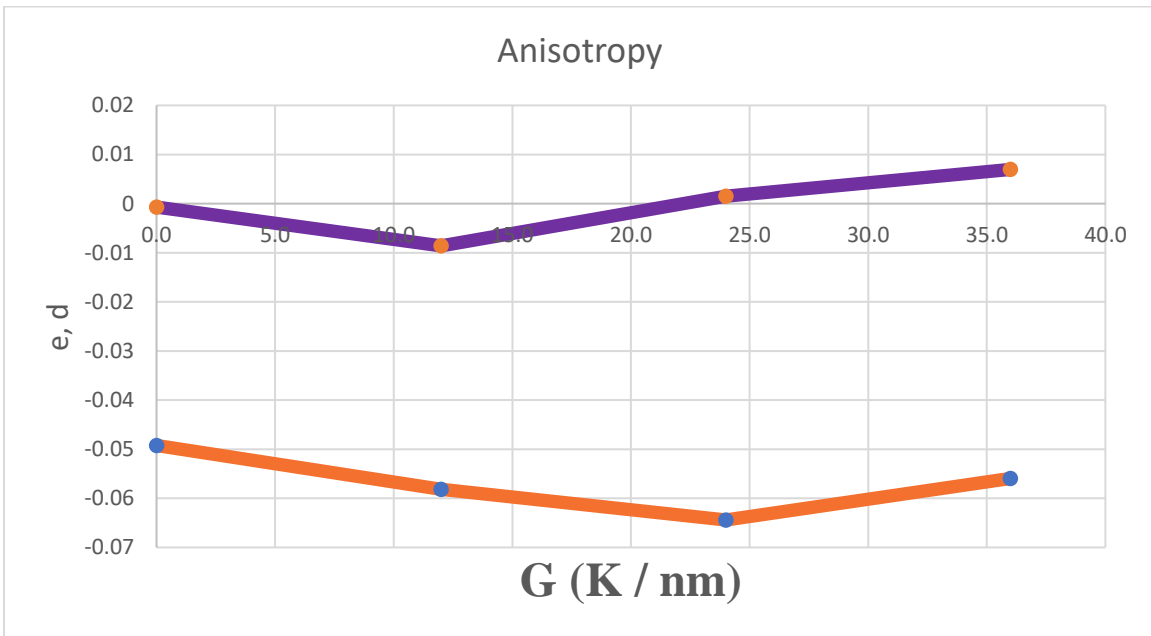

Figure 10: Temprature gradient (K) versus anisotropy parametrs for Temprature 905

In light of the assumption that the anisotropy of the solid-liquid interface remains unaffected by the thermal gradient, we employ the e and d parameters, which are determined under conditions of equilibrium, to calculate the interfacial free energy for each orientation. The equations specified in Table 7 are utilized for this purpose. A linear relationship between interfacial energy and temperature gradient is observed by calculating the average interfacial energy across various orientations, as illustrated in Figure 9 This allows for the determination of an energy function for the Al-Cu alloy, denoted as $\gamma_{(\theta,G)} = \mu G + \gamma_0$ where γ_0 represents the interfacial free energy when the system is in a state of thermal equilibrium and $\mu = 0.552 \frac{m \cdot J \cdot nm}{m^2 k}$. In order to validate the hypothesis that material anisotropy remains unaltered by temperature gradients, we replicate the equilibrium-based methodologies for calculating the parameters that are dependent on gradients, as illustrated in Figure 10. After conducting an analysis of the anisotropy parameters, it becomes apparent that there is no observable correlation between anisotropy and temperature gradient.

In light of our initial assumption regarding the relationship between interfacial stiffness and a second-order Taylor expansion of interfacial energy, as presented in Equation (16), it is evident that the inclusion of higher-order terms can be neglected when considering Al-Cu alloys. This is due to the linear nature of the energy-gradient relationship in this particular case. Therefore, the theoretical definition of the solid-liquid interfacial stiffness for Al-Cu can be expressed as $S_{(\theta,G)} = \gamma + \gamma_{\theta\theta} + \mu G$. The findings from the molecular dynamics (MD) simulations demonstrate a significant correlation with the proposed theoretical framework, thus confirming the validity of the assumptions made

regarding gradient-independent anisotropy parameters and the utilization of a first-order Taylor expansion to approximate interfacial energy. As the sample size is increased by incorporating additional random seed numbers, it is expected that the discrepancy between the theoretical predictions and the results obtained from the simulation will progressively decrease.

Table 12: Interfacial stifness of eight orientation at 905K

905								
Gradient	100[001]	110[-110]	110[001]	110[1-10]	111[-1-12]	111[1-10]	120[001]	120[2-10]
0	54.05	47.11	53.60	49.84	43.91	42.60	43.15	52.86
12	75.68	55.80	57.99	51.95	46.18	49.58	52.35	64.56
24	69.24	69.01	76.15	66.98	53.08	53.06	52.86	82.29
36	76.66	87.45	92.14	88.79	57.23	70.87	65.16	96.31

Figure 11: Graphical representation Interfacial stiffness of eight orientation plotted against thermal gradient at 905K

Table 13: Interfacial stifness of eight orientation at 888K

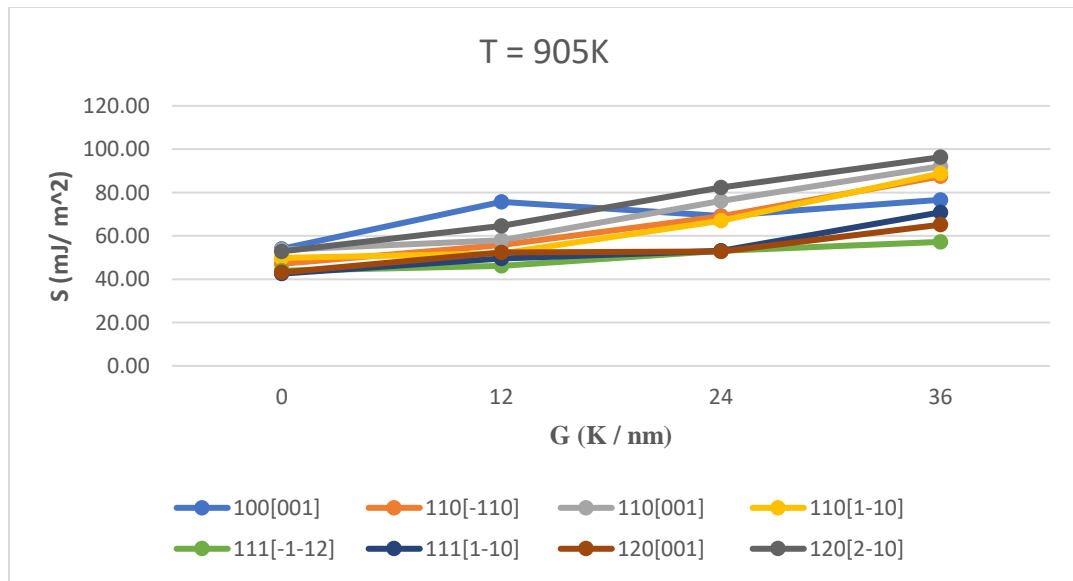| 888 Gradient	100[001]	110[-110]	110[001]	110[1-10]	111[-1-12]	111[1-10]	120[001]	120[2-10]
0	47.41	34.84	44.83	40.53	35.10	39.58	34.67	41.83
12	51.35	40.54	43.98	44.17	47.75	42.45	38.63	43.16
24	52.68	44.02	50.23	41.39	42.93	41.56	38.89	49.27
36	58.79	44.64	53.08	49.65	47.33	48.70	42.89	43.01

Figure 12: Graphical representation Interfacial stiffness of eight orientation plotted against thermal gradient at 888K

Table 14: Interfacial stifness of eight orientation at 874K

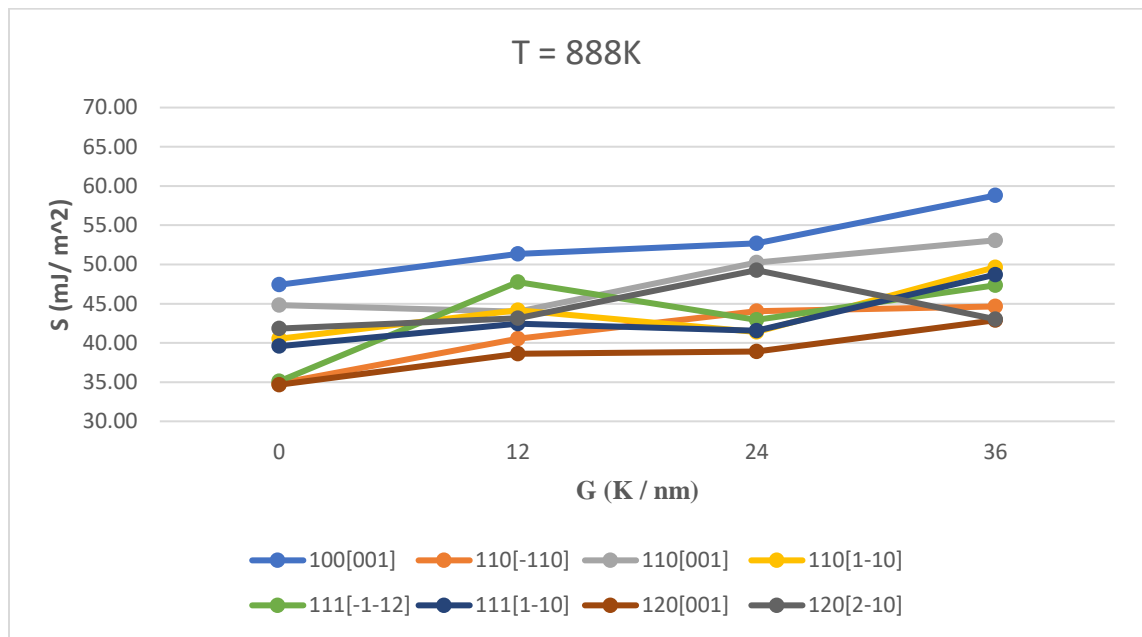| 874 Gradient	100[001]	110[-110]	110[001]	110[1-10]	111[-1-12]	111[1-10]	120[001]	120[2-10]
0	32.50	27.31	28.60	31.40	25.81	22.33	14.02	30.28
12	31.09	27.59	28.50	29.46	27.19	22.76	18.71	28.98
24	48.92	27.92	27.44	27.75	25.22	27.38	18.11	26.83
36	50.52	29.87	34.43	29.56	27.27	26.60	23.09	32.47
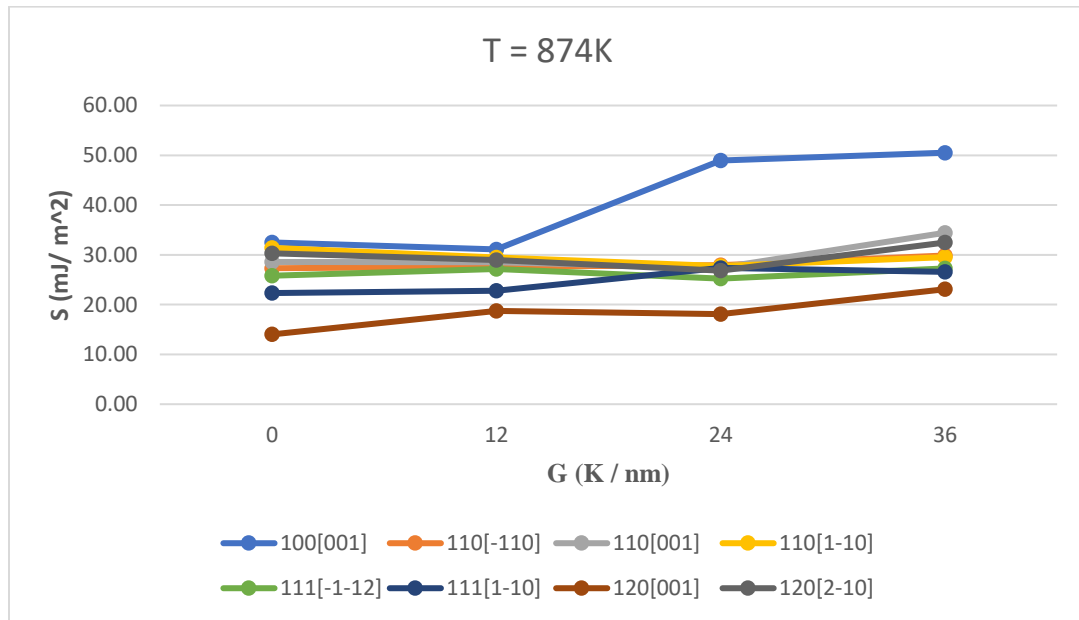
Figure 13: Graphical representation Interfacial stiffness of eight orientation plotted against thermal gradient at 874K

The results obtained from the molecular dynamics (MD) simulations demonstrate a significant level of concurrence with the theoretical hypothesis. This finding provides support for the underlying assumptions of gradient-independent anisotropy parameters and the utilization of a first-order Taylor expansion to model interfacial energy. It is crucial to acknowledge that through the inclusion of supplementary random seed numbers in the sampling process, we expect a further reduction in the disparity between theoretical predictions and simulation results. This will serve to strengthen the reliability and effectiveness of our methodology.

The effective determination of the two-phase interface within the Al-Cu FCC structure can be achieved by employing either the centrosymmetry parameter. In this

research, we utilized this approach to ascertain the interface, as illustrated in Figure 14, in accordance with the methodology described in chapter 2.
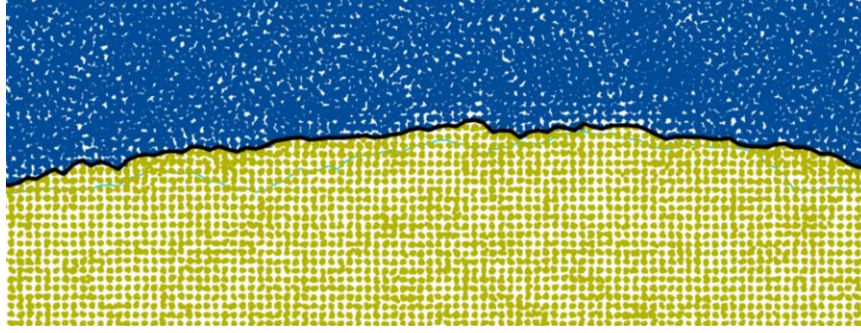
Figure 14: Al-Cu solid-liquid interface defined using a bin size of 2.1x2.1A (Centrosymetry parameter)

After obtaining time-history records of the interface height over a thousand configurations, we interpolate the interface length for every configuration, enlarging it to include 5,000 data points. We then use Fourier series methods to calculate the relevant numbers $\langle |A(k)|^2 \rangle$ stiffness is defined as $(\gamma + \gamma_{\theta\theta}) = \frac{k_B T m}{bw\langle |A \cdot (k)|^2 \rangle k^2}$ and can be extracted as slope of a $\frac{k_B T m}{bw\langle |A \cdot (k)|^2 \rangle k^2}$ versus k^2 for our investigation.

To be more precise, the Capillary Fluctuation method (CFM) uses Fourier analysis to identify interface height fluctuations and relates these fluctuations to an interfacial stiffness parameter. It is crucial to remember that this method's validity depends on the assumption of tiny fluctuations, which is a key component in its derivation. However, if the bin size is defined to be much smaller than the lattice parameter, then this assumption may be called into question.

We have conducted an investigation to examine the possible influence of the sharp peaks in the interface height on the computed stiffness. In particular, as Figure 15 shows,

we have established a range of bin widths that extend from 2.1 to 8.4 angstroms. Then, we use the CFM to determine the corresponding stiffness in these different bin width scenarios. This analysis attempts to clarify the potential effects of bin width selection on computed stiffness values.
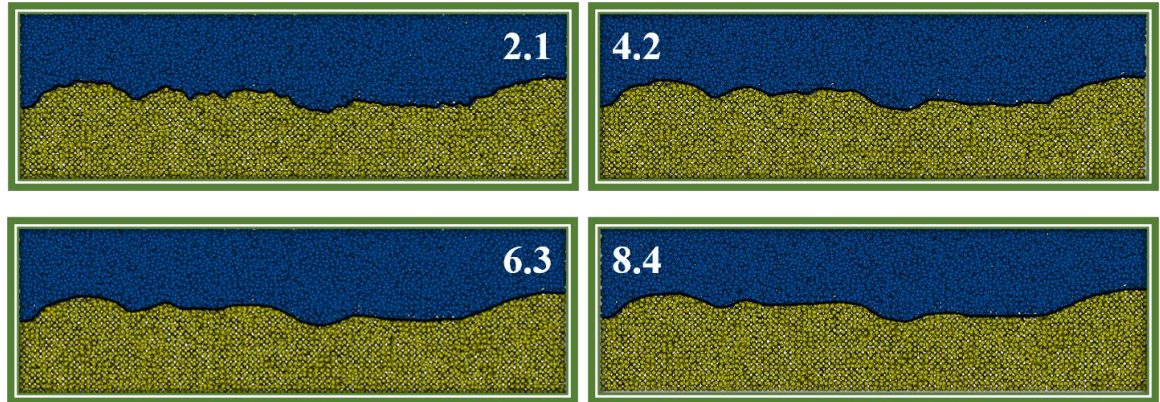
Figure 15: Interface dimensions defined by varying bin widths from 2.1-8.4 angstroms

4.2 Conclusion

In this study, I have dedicated my efforts to investigating the characteristics of the solid-liquid interface in Al-Cu alloy using molecular dynamics (MD) simulations in conjunction with the capillary fluctuation method (CFM). I employed the CFM to compute interfacial properties like energy, stiffness, and anisotropy under equilibrium conditions and thermal gradient, which are representative of rapid solidification processes such as casting, additive manufacturing and laser welding.

The introduction of a temperature gradient across the interface led to an augmentation of stiffness and energy properties while maintaining anisotropic features. The underlying rationale for these heightened parameters can be theoretically elucidated through a second order Taylor expansion of interfacial free energy and the derivation of

the system's energy at the solid-liquid interface. The resultant equations for energy and stiffness are expressed as $\gamma_{(\theta,G)} = \mu G + \gamma_0$ and $S_{(\theta,G)} = \gamma + \gamma_{\theta\theta} + \mu G$ respectively. For the EAM-modeled Al-Cu discussed in this research, the values are (mu and stiffness)

While published sources indicate typical gradients for additive manufacturing processes in the range of 10^3 to 10^5 K/mm [33,34], these figures are often estimated at larger scales through finite element analysis (FEA) approaches and may not precisely represent the gradient at the atomic level. MD simulations are constrained to a length scale on the order of nanometers, which, in turn, limits the applied temperature gradient. Nevertheless, this study establishes a relationship between temperature gradient and stiffness and energy, which can be used for further computational applications.

The results indicate that temperature gradients across the solid-liquid interface, which simulate conditions of rapid solidification, have the potential to substantially alter the interface's properties. Therefore, when conducting dendrite growth phase-field simulations and utilizing the Gibbs-Thomson condition to calculate the temperature at the interface, assuming equilibrium conditions for systems characterized by extreme rates of heating and cooling may prove to be an erroneous assumption. At high interface velocities, this may be a contributing factor to the imprecision of phase-field geometric representations. The integration of non-equilibrium thermal conditions into multi-scale computational methods presents an opportunity to initiate the process of reconciling the discrepancy between computational model predictions and inconsistent experimental material strength outcomes.

In conclusion, this study has employed molecular dynamics simulations to illustrate the impact of thermal gradients on the properties of solid-liquid interfaces, suggesting a deviation from the state of equilibrium. The implications of the findings are significant for computational models utilized in rapid solidification processes such as additive manufacturing. The inclusion of non-equilibrium conditions has the potential to enhance the level of correlation observed between models and experimental data. Additional research could involve expanding the analysis to encompass various materials and a wider range of gradients.

Chapter Five

5.1 Conclusion

This thesis employs molecular dynamics (MD) simulations to investigate the characteristics of solid-liquid interfaces in aluminum-copper (Al-Cu) alloys under thermal gradients representative of rapid solidification processes like additive manufacturing.

The motivation stems from the need to better understand interface behavior during rapid solidification to optimize manufacturing processes and computational models. Conventional phase-field simulations rely on a Gibbs-Thomson condition derived under equilibrium that may not apply under dynamic non-equilibrium conditions with high heating/cooling rates. MD simulations at the atomic scale complement experiments and provide input to mesoscale models.

The literature review covers key concepts like normal versus rapid solidification, dendrite growth patterns, the continuum growth model of solute trapping, and phase-field modeling approaches. It highlights limitations of assuming local equilibrium at high solidification front velocities and introduces the capillary fluctuation method (CFM) for computing interface properties.

MD principles are outlined including Newton's equations of motion, integration algorithms like Velocity Verlet, interatomic potentials, and ensemble types. CFM relates stiffness to fluctuations in interface height through statistical mechanics. Weak anisotropy in crystalline materials is described by a harmonic expansion of the interface energy.

Simulations were performed with a modified embedded-atom method potential optimized for Al-Cu alloys. Two-phase structures were created by cooling to an

equilibrium melting temperature with proper thermostatting and barostatting protocols. Thermal gradients were then applied by bounding dynamic Langevin thermostat regions while maintaining a stationary interface.

CFM required precisely locating the interface from atom positions. This was accomplished by binning centrosymmetry parameters and locating the point of maximum difference between solid and liquid phases. Fourier analysis extracted fluctuations in interface height profiles over multiple configurations.

The key results demonstrate that thermal gradients augment the interface stiffness and free energy while maintaining inherent anisotropic properties. This matches a theoretical model using a second-order Taylor expansion of the interface free energy function. The relationships derived are: $\gamma_{(\theta,G)} = \mu G + \gamma_0$ for energy and $S_{(\theta,G)} = \gamma + \gamma_{\theta\theta} + \mu G$ for stiffness.

Three Al-Cu alloys were simulated at different temperatures, 2% Cu at 905K, 3.58% Cu at 888K, and 5.065% Cu at 874K. Eight distinct interface orientations were examined. The stiffness, energy, and anisotropy parameters were calculated at gradients from 0 to 36 K/nm. Outcomes aligned with theory, proving anisotropy persists independent of the gradient.

This study provides a rigorous methodology for analyzing solid-liquid interface properties under non-equilibrium conditions relevant to manufacturing. The results have significant implications for more accurate phase-field and computational modeling of rapid solidification processes by considering thermal effects. Incorporating non-equilibrium

interface parameters will enhance correlation with experimental microstructures and defect observations.

5.2 Future Work

This study has provided fundamental insights into the behavior of solid-liquid interfaces in Al-Cu alloys under thermal gradients representative of rapid solidification processes. However, there are several promising avenues for extending this work further:

Investigate a broader range of thermal gradients: In this study, gradients up to 36 K/nm were examined due to computational constraints at the nanoscale inherent to MD simulations. Applying steeper gradients closer to experimental measurements would provide greater insight. This could potentially be achieved through larger simulation sizes or advanced sampling techniques.

Incorporate solute trapping effects: The accumulation of solute atoms at the advancing solidification front is a phenomenon prevalent in rapid solidification that was not accounted for here. Introducing a solute species like Cu into the liquid phase could reveal impacts on interfacial properties.

Explore alternate interatomic potentials: The results obtained are inherently dependent on the empirical potential used. Comparing outcomes from additional EAM, MEAM or other many-body potentials could improve reliability. This may require recalibrating potentials to experimental data.

Examine alternative materials: Expanding the analysis to other alloy systems and pure metals would allow broader application and comparison. Metals like steel, nickel and titanium alloys have relevance to additive manufacturing.

Relate parameters to mesoscale models: The interface properties calculated could serve as inputs to phase-field simulations of microstructure evolution. Quantifying the effects on dendrite morphology and defect formation would bridge scales.

Compare to in situ experimental characterization: Recent advances allow dynamic experimental measurement of solid-liquid interfaces. Relating simulations and experiments would provide validation and refine computational methods.

In summary, this work has established a rigorous methodology for analyzing solid-liquid interfaces using MD and CFM under equilibrium conditions. Progressing along these proposed directions will further improve physics-based modeling of rapid solidification processes and enhance our fundamental understanding of interfacial phenomena. More reliable computational representations will ultimately accelerate the development of materials for advanced manufacturing technologies.

REFERENCES

References

[1] Pal, P., and Phillion, A. B., 2022, "Predicting Solid−liquid Interfacial Characteristics during Rapid Solidification," Computational Materials Science, **213**pp. 111629.

[2] Kurz, W., and Trivedi, R., 1994, "Rapid Solidification Processing and Microstructure Formation," Materials Science and Engineering: A, **179-180**pp. 46-51.

[3] Anderson, I., and Rath, B., 1985, "Rapid Solidification of Copper-Based Alloys, Paper from the TMS-AIME Northeast Regional Meeting, Rapidly Solidified Crystalline Alloys, Morristown, New Jersey, may 1-3, 1985," TMS Papers, pp. 219-244.

[4] Hoyt, J. J., Asta, M., and Karma, A., 2003, "Atomistic and Continuum Modeling of Dendritic Solidification," Materials Science & Engineering. R, Reports : A Review Journal, **41**(6) pp. 121-163.

[5] Karma, A., and Rappel, W., 1998, "Quantitative Phase-Field Modeling of Dendritic Growth in Two and Three Dimensions," Physical Review. E, Statistical Physics, Plasmas, Fluids, and Related Interdisciplinary Topics, **57**(4) pp. 4323-4349.

[6] Tourret, D., Clarke, A. J., Imhoff, S. D., 2015, "Three-Dimensional Multiscale Modeling of Dendritic Spacing Selection during Al-Si Directional Solidification," Jom, **67**(8) pp. 1776-1785.

[7] Gurevich, S., Amoorezaei, M., and Provatas, N., 2010, "Phase-Field Study of Spacing Evolution during Transient Growth," Physical Review. E, Statistical, Nonlinear, and Soft Matter Physics, **82**(5 Pt 1) pp. 051606.

[8] Karma, A., and Tourret, D., 2016, "Atomistic to Continuum Modeling of Solidification Microstructures," Current Opinion in Solid State and Materials Science, **20**(1) pp. 25-36.

[9] Nie, P., Ojo, O. A., and Li, Z., 2014, "Numerical Modeling of Microstructure Evolution during Laser Additive Manufacturing of a Nickel-Based Superalloy," Acta Materialia, **77**pp. 85-95.

[10] Mishin, Y., 2004, "Atomistic Modeling of the Γ and Γ '-Phases of the Ni−Al System," Acta Materialia, **52**(6) pp. 1451-1467.

[11] Cheng, B., Tribello, G., and Ceriotti, M., 2015, "Solid-Liquid Interfacial Free Energy Out of Equilibrium," Physical Review. B, **92**(18) .

[12] Hoyt, J. J., Asta, M., and Karma, A., 2001, "Method for Computing the Anisotropy of the Solid-Liquid Interfacial Free Energy," Physical Review Letters, **86**(24) pp. 5530-5533.

[13] Brown, N. T., 2017, "Molecular Dynamics Simulations of Interfaces in Thin Films and Rapid Solidification," .

[14] Kolb, T., Gebhardt, P., Schmidt, O., 2018, "Melt Pool Monitoring for Laser Beam Melting of Metals: Assistance for Material Qualification for the Stainless Steel 1.4057," Procedia CIRP, **74**pp. 116-121.

[15] Becker, C. A., Olmsted, D., Asta, M., 2007, "Atomistic Underpinnings for Orientation Selection in Alloy Dendritic Growth," Physical Review Letters, **98**(12) pp. 125701.

[16] Anonymous "Https://Www.Wikiwand.Com/En/AlCu?Cv=1," .

[17] Ziaeetabar, F., "Spatio-Temporal Reasoning for Semantic Scene Understanding and its Application in Recognition and Prediction of Manipulation Actions in Image Sequences," .

[18] Rapaport, D.C., 1997, "Theœart of molecular dynamics simulation," Univ. Press, Cambridge [u.a], .

[19] Anonymous "J. Haile, Molecular Dynamics Simulation, Wiley, New York1992." .

[20] Swope, W. C., Andersen, H. C., Berens, P. H., 1982, "A Computer Simulation Method for the Calculation of Equilibrium Constants for the Formation of Physical Clusters of Molecules: Application to Small Water Clusters," The Journal of Chemical Physics, **76**(1) pp. 637-649.

[21] Anonymous 2004, "Computational Soft Matter: From Synthetic Polymers to Proteins ; NIC Winter School, 29 February - 6 March 2004, Gustav-Stresemann-Institut, Bonn, Germany - Lecture Notes," .

[22] Plimpton, S., 1995, "Fast Parallel Algorithms for Short-Range Molecular Dynamics," Journal of Computational Physics, **117**(1) pp. 1-19.

[23] Davidchack, R. L., Morris, J. R., and Laird, B. B., 2006, "The Anisotropic Hard-Sphere Crystal-Melt Interfacial Free Energy from Fluctuations," The Journal of Chemical Physics, **125**(9) pp. 094710.

[24] Hoyt, J. J., Asta, M., and Karma, A., 2001, "Method for Computing the Anisotropy of the Solid-Liquid Interfacial Free Energy," Physical Review Letters, **86**(24) pp. 5530-5533.

[25] Hoyt, J. J., Trautt, Z. T., and Upmanyu, M., 2010, "Fluctuations in Molecular Dynamics Simulations," Mathematics and Computers in Simulation, **80**(7) pp. 1382-1392.

[26] KARMA, A., 1993, "Fluctuations in Solidification," Physical Review. A, Atomic, Molecular, and Optical Physics, **48**(5) pp. 3441-3458.

[27] Asadi, E., Asle Zaeem, M., Nouranian, S., 2015, "Two-Phase Solid−liquid Coexistence of Ni, Cu, and Al by Molecular Dynamics Simulations using the Modified Embedded-Atom Method," Acta Materialia, **86**pp. 169-181.

[28] Fehlner, W. R., and Vosko, S. H., 1976, "A Product Representation for Cubic Harmonics and Special Directions for the Determination of the Fermi Surface and Related Properties," Canadian Journal of Physics, **54**(21) pp. 2159-2169.

[29] Plimpton, S., 1995, "Fast Parallel Algorithms for Short-Range Molecular Dynamics," Journal of Computational Physics, **117**(1) pp. 1-19.

[30] Cai, J., and Ye, Y., 1996, "Simple Analytical Embedded-Atom-Potential Model Including a Long-Range Force for Fcc Metals and their Alloys," Physical Review. B, Condensed Matter, **54**(12) pp. 8398-8410.

[31] Mendelev, M. I., Kramer, M. J., Becker, C. A., 2008, "Analysis of Semi-Empirical Interatomic Potentials Appropriate for Simulation of Crystalline and Liquid Al and Cu," Philosophical Magazine (Abingdon, England), **88**(12) pp. 1723-1750.

[32] Azizi, G., Kavousi, S., and Asle Zaeem, M., 2022, "Interactive Effects of Interfacial Energy Anisotropy and Solute Transport on Solidification Patterns of Al-Cu Alloys," Acta Materialia, **231**pp. 117859.

[33] Asadi, E., Asle Zaeem, M., Nouranian, S., 2015, "Two-Phase Solid−liquid Coexistence of Ni, Cu, and Al by Molecular Dynamics Simulations using the Modified Embedded-Atom Method," Acta Materialia, **86**pp. 169-181.

[34] Levi, C. G., and Mehrabian, R., 1982, "Heat Flow during Rapid Solidification of Undercooled Metal Droplets," Metallurgical Transactions. A, Physical Metallurgy and Materials Science, **13**(2) pp. 221-234.

[35] HERLACH, D. M., 1994, "Non-Equilibrium Solidification of Undercooled Metallic Melts," Materials Science & Engineering. R, Reports : A Review Journal, **12**(4-5) pp. 177-272.

[36] Brown, N. T., Martinez, E., and Qu, J., 2017, "Interfacial Free Energy and Stiffness of Aluminum during Rapid Solidification," Acta Materialia, **129**(C) pp. 83-90.

APPENDICES
Table A.1 Calculated stifeness for equilibrium at all thermal graidents

Case		$\gamma+\gamma''/\gamma 0$	Equilibrium $\gamma+\gamma''$	Calculated $\gamma+\gamma''$	error	12K/nm $\gamma+\gamma''$	Calculated $\gamma+\gamma''$	error	24K/nm $\gamma+\gamma''$	Calculated $\gamma+\gamma''$	error	36K/nm $\gamma+\gamma''$	Calculated $\gamma+\gamma''$	error
1	100[010]	1-3.6e-11.4d	55	55	0.0%	76	76	0%	69	69	0%	77	77	0%
2	110[001]	1+3.9e+11.1d	54	37	31.4%	58	39	32%	76	44	43%	92	59	36%
3	110[1-10]	1-2.1e+26.1d	50	50	0.0%	52	52	0%	67	67	0%	89	89	0%
5	110[-110]	1-2.1e+26.1d	47	50	-5.8%	56	52	7%	69	67	3%	87	89	-2%
6	111[1-10]	1-2.4e-20.3d	43	52	-22.3%	50	76	-53%	53	64	-21%	71	68	4%
7	111[-1-12]	1+9e-9.4d	44	26	41.0%	46	32	30%	53	23	56%	57	29	49%
8	120[001]	1+1.2e+3d	43	43	0.0%	52	52	0%	53	53	0%	65	65	0%
9	120[2-10]	1-2.64e+12.6d	53	52	2.5%	65	61	6%	82	68	18%	96	84	12%